PROCEEDINGS, 51st Workshop on Geothermal Reservoir Engineering
Stanford University, Stanford, California, February 9-11, 2026
SGP-TR-230

Comprehensive Laboratory Measurements of the Hydraulic and Electrical Conductivities of Electrically Conductive Proppant-Supported Fractures under Enhanced Geothermal System Conditions

Shuo Wang[1], Parisa Bazazi[2], Jennifer Miskimins[2], Carlos Torres-Verdín[3], and Cheng Chen[1*]

[1]Department of Civil, Environmental and Ocean Engineering, Stevens Institute of Technology, Hoboken, NJ 07030, United States

[2]Department of Petroleum Engineering, Colorado School of Mines, Golden, CO 80401, United States

[3]Hildebrand Department of Petroleum and Geosystems Engineering, The University of Texas at Austin, Austin, TX 78712, United States

* Corresponding author: cchen6@stevens.edu

Keywords: Enhanced geothermal systems; High-temperature; Electrically-conductive proppants; Hydraulic conductivity; Electrical conductivity

ABSTRACT

Hydraulic fracturing with proppants in enhanced geothermal systems (EGS) improves reservoir permeability, thereby enhancing the efficiency and economic viability of geothermal energy recovery. Accurate fracture diagnostics remain critical for the long-term success of EGS projects. Borehole electromagnetic measurements using electrically-conductive (EC) proppants and fluids provide a promising approach for mapping fractures and proppant distribution. To evaluate the effect of using EC proppants under EGS conditions, we conducted comprehensive measurements of the hydraulic and electrical conductivities of EC proppant-supported fractures under stress and temperature conditions typical of the Utah-FORGE EGS. EC proppants of 30/50-mesh and 40/70-mesh sizes were placed in the space between two Sierra White granite slabs and then subjected to confining stresses up to 10,000 psi and the temperature of 230 °C. Hydraulic conductivity of the EC proppant-supported fracture, defined as the product of fracture permeability and fracture width, was measured under various confining stresses and proppant concentrations. The proppant concentration is defined as the proppant mass per unit fracture-face area. The results revealed non-monotonic dependence of the fracture hydraulic conductivity on the proppant concentration. These findings indicate that significant fracture hydraulic conductivity can be achieved using a partial-monolayer proppant pack in granite fractures, underscoring the potential for reducing material costs. Measurements under dry conditions show that EC proppant-supported fractures exhibit increasing electrical conductivity with confining stress due to enhanced interparticle contacts. It establishes a benchmark for electrical conductivity of EC proppant-supported fractures, which serves as a reference for subsequent measurements under brine-saturated conditions. These comprehensive laboratory testing data highlight the potential of using EC proppants in field-scale EGS fracture diagnostics.

1. INTRODUCTION

The rising global energy demand, together with mounting environmental challenges, has made the transition from fossil fuels to clean and renewable energy a widely recognized long-term objective. Compared with other renewable energy sources such as wind, solar, biomass, and hydropower, geothermal energy has attracted considerable attention due to its non-intermittent nature and substantial subsurface heat potential, thereby providing stable and continuous baseload power generation (Nataša A. Kablar, 2019; Szanyi et al., 2023; Meng et al., 2025). Naturally occurring geothermal systems require three essential elements: heat, fluids, and sufficient permeability to enable fluid circulation and energy extraction (Jolie et al., 2021). However, in many regions, substantial geothermal resources are hosted in hot dry rock formations characterized by high temperatures but limited natural permeability and fluid availability (Tomac and Sauter, 2018; Jolie et al., 2021). To overcome these limitations and fully utilize such geothermal resources, enhanced geothermal systems (EGS) employ engineered reservoir stimulation to reactivate pre-existing natural fractures and create artificial fracture networks, thereby enabling fluid circulation, enhancing permeability, and achieving efficient heat extraction (Al Balushi et al., 2023; Nath et al., 2024).

At the depths relevant to enhanced geothermal systems, fractures within hot dry rock are subjected to large confining stresses, which tend to progressively close fractures or significantly reduce their hydraulic conductivity (Li et al., 2019, 2020; Al Balushi et al., 2023). In engineering practice, hydraulic stimulation techniques are commonly employed, in which proppants, such as ceramic materials, are injected with fracturing fluids to keep fractures open and provide sufficient hydraulic conductivity for sustained fluid flow (Li et al., 2016; Li et al., 2025). Importantly, the primary objective of stimulation in enhanced geothermal systems is not merely to improve fluid circulation, but to extract heat at higher rates (Gan and Elsworth, 2016; Liang et al., 2025; Zhang et al., 2025). Extensive field observations and numerical analyses indicate that, despite the presence of complex fracture networks, fluid flow often localizes into only a limited number of fractures or effectively short-circuits between injection and production wells (Li et al., 2024; Liu et al., 2025). Such preferential flow pathways significantly reduce the effective heat exchange area and, consequently, the overall heat extraction efficiency (Gong et al., 2020; Li et al., 2024).

Accordingly, optimizing fracture treatment design requires accurate characterization of mapping fracture development and proppant distribution (Zhang et al., 2021). To this end, a variety of diagnostic and monitoring techniques have been developed to characterize

fracture geometry and evolution. However, their capability to resolve proppant distribution throughout the fracture network remains highly limited. Existing methods either cannot directly assess proppant placement, such as micro-seismic imaging and acoustic logging, or are largely restricted to only near-wellbore characterization of proppant distribution, such as proppant tracers and fiber-optic surveys (Palisch et al., 2017; Zhang et al., 2021). Nevertheless, the characterization of proppant distribution throughout the fracture network is critical not only for fracture treatment optimization, but also for well spacing design and perforation cluster placement, which together play a key role in enhancing reservoir performance over the entire life cycle of enhanced geothermal systems (Palisch et al., 2017; Zhang et al., 2021; Qu et al., 2024; Ren et al., 2025).

Electromagnetic (EM) borehole measurement methods have been proposed to map fracture development and proppant distribution throughout fracture networks by exploiting changes in electric and/or magnetic field responses associated with electrically-conductive (EC) proppants in resistive formations (Hoversten and Schwarzbach, 2021; Zhang et al., 2021; Wu et al., 2024). When a large electrical conductivity contrast exists between EC proppants and resistive formations, the detection and characterization of proppant-supported fractures are enhanced. Accordingly, EC proppant particles have been developed to achieve conductivity contrasts of several orders of magnitude relative to the host formation (Palisch et al., 2017). Existing studies related to proppants in enhanced geothermal systems can be broadly categorized into two research directions. On one hand, EC proppants have been investigated for electromagnetic-based fracture diagnostics, demonstrating their potential for estimating proppant-supported fracture volumes and supporting EM measurements (Hoversten and Schwarzbach, 2021; Zhang et al., 2021). On the other hand, proppant behavior in enhanced geothermal systems has been examined primarily from a thermal and mechanical perspective, with a focus on heat extraction and thermal breakthrough behavior, as well as proppant mechanical performance under high-temperature conditions (Al Balushi et al., 2023; Balushi and Taleghani, 2023; Ko et al., 2023). However, the comprehensive laboratory tests on the fracture hydraulic and electrical conductivities of EC proppants under EGS-relevant temperature and stress have not yet been systematically reported. Moreover, the reported material costs of EC proppants remain prohibitively high.

In this study, we conducted well-controlled comprehensive laboratory experiments under stress and temperature conditions typical of the Utah-FORGE enhanced geothermal system (EGS) to investigate the hydraulic and electrical conductivities of EC proppant-supported fractures against proppant concentration, ranging from 0 to 2 lb/ft². The measurements of fracture hydraulic conductivity were performed to evaluate the ability of EC proppants to maintain hydraulic conductivity and provide effective fracture support during fluid circulation. The measurements of fracture were conducted to quantify fracture electrical conductivity of EC proppant-supported fractures and support the field-scale application of borehole electromagnetic (EM) measurements in enhanced geothermal systems.

2. METHODS AND MATERIALS

2.1 Laboratory equipment and materials

Figure 1 illustrates the equipment used for measuring fracture hydraulic and electrical conductivities, including a measurement cell, in which proppant particles were placed between two Sierra White granite slabs. All Sierra White granite slabs used in the experiments had dimensions of 7 inches in length, 1.5 inches in width, and 0.5 inch in thickness, and were cored from the same parent rock block to ensure comparable initial mechanical properties. Two sizes of iON electrically-conductive proppants, 30/50-mesh and 40/70-mesh, were employed in the experiments. During the experiments, the closure stress was applied up to 10,000 psi with a precision of 0.2%, and an electrical heater maintained a testing temperature of 230 °C with a precision of 0.4%, corresponding to stress and temperature conditions typical of the Utah-FORGE enhanced geothermal system.

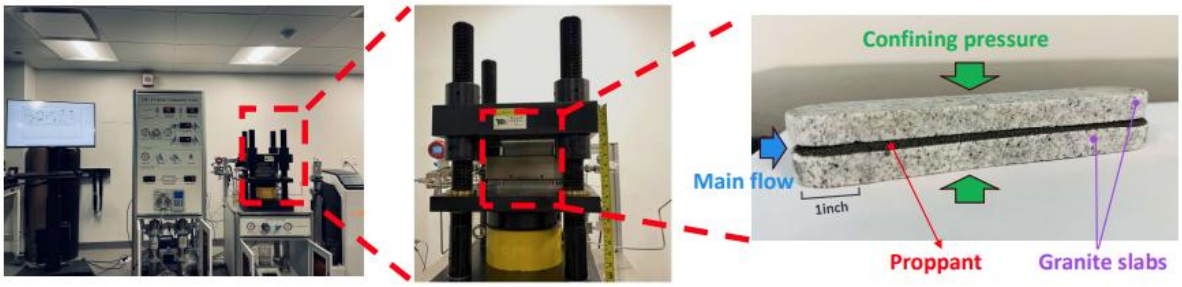

Figure 1: Experimental setup for measuring fracture hydraulic and electrical conductivities. The system includes a measurement cell in which proppant particles are placed between two Sierra White granite slabs and subjected to confining stress.

2.2. Hydraulic conductivity measurements

Hydraulic conductivity measurements were conducted to investigate the effects of proppant packing structure and effective stress on the hydraulic conductivity of EC proppant-supported fractures. A range of proppant concentrations was tested for the two proppant sizes described above to represent different packing conditions. The proppant concentration within the fracture was determined based on the proppant mass and the surface area of the rock slabs, and this definition was used for the measurements of both hydraulic and electrical conductivities. For 40/70-mesh proppants, concentrations of 0.06 lb/ft² (a partial-monolayer proppant pack), 0.16 lb/ft² (a full-monolayer proppant pack), and 1 and 2 lb/ft² (multilayer proppant packs) were tested. For 30/50-mesh proppants, concentrations of 0.06 lb/ft² (a partial-monolayer proppant pack), 0.22 lb/ft² (a full-monolayer proppant pack), and 1 and 2 lb/ft² (multilayer proppant packs) were tested. The partial-monolayer proppant concentration of 0.06 lb/ft² was selected based on prior experimental and numerical studies that identified

characteristic proppant concentrations associated with optimized fracture hydraulic conductivity (Fan et al., 2019; Li et al., 2022). Five effective stress levels ranging from 2,000 to 10,000 psi, in increments of 2,000 psi, were applied in the measurements of fracture hydraulic conductivity.

The hydraulic conductivity of a fracture, C, is defined as the flow rate contributed by a unit length of fracture. Accordingly, C, is calculated as:

$$C = kw_f = \frac{\mu \cdot Q \cdot L \cdot w_f}{\Delta p \cdot A} = \frac{\mu \cdot Q \cdot L}{\Delta p \cdot h} \quad (1)$$

where C is the fracture hydraulic conductivity (m^3); k is the fracture permeability (m^2); w_f is the fracture width (m); h is the size of the longer dimension of the fracture cross section (m); A is the area of fracture cross section and equal to $w_f \cdot h$ (m^2); μ is the fluid viscosity (Pa·s); Q is the flow rate (m^3/s); L is the length over which the pressure difference is measured (m); Δp is the pressure difference (Pa). Note that μ, L, and h in Equation (1) are known. The measured flow rate, Q, and pressure difference, Δp, are then imported into Equation (1) to calculate the fracture hydraulic conductivity.

2.3. Electrical conductivity measurements

Electrical conductivity measurements were conducted to investigate the effects of proppant packing structure and effective stress on the electrical conductivity of EC proppant-supported fractures. Measurements were performed using the same measurement cell described above, integrated with an LCR meter to measure the electrical resistance of the EC proppant-supported fracture. A four-point probe method, as shown in Figure 2, was adopted to effectively minimize the influence of electrode and lead contact resistance (Zhang et al., 2021; Suzuki et al., 2024). During testing, a 60-Hz AC current was applied through the current electrodes, which were electrically isolated from the measurement cell, while additional electrical insulation tape was used to isolate the EC proppant-supported fracture region from surrounding cell components, thereby minimizing unintended current leakage paths.

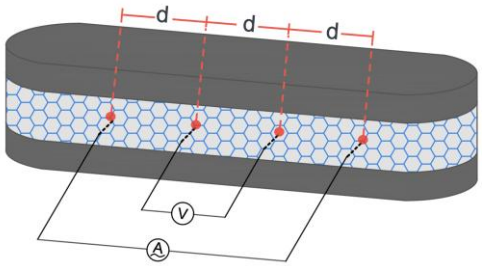

Figure 2: Schematic plot of the four-point probe method used for electrical conductivity measurements of an EC proppant-supported fracture.

A range of proppant concentrations was tested for the two proppant sizes described above to represent different packing conditions. For 40/70-mesh proppants, concentrations of 0.16 lb/ft² (a full-monolayer proppant pack) and 1 and 2 lb/ft² (multilayer proppant packs) were tested. For 30/50-mesh proppants, concentrations of 0.22 lb/ft² (a full-monolayer proppant pack) and 1 and 2 lb/ft² (multilayer proppant packs) were tested. Confining stress levels ranging from 1,000 to 10,000 psi, applied at increments of 1,000 psi, were used during the electrical conductivity measurements.

The electrical resistivity of an EC proppant-supported fracture, ρ, was calculated from the measured fracture resistance, R, using the fracture cross-sectional area A and a fixed electrode spacing, d, according to Equation (2):

$$\rho = \frac{R \cdot A}{d} \quad (2)$$

where ρ is the fracture electrical resistivity (Ω·m), R is the measured electrical resistance of the fracture (Ω), d is the electrode spacing (m). The fracture electrical conductivity, σ (S/m), is calculated as the reciprocal of the fracture electrical resistivity ρ.

3. RESULTS AND DISCUSSION

3.1 Hydraulic conductivity

As shown in Figure 3, the hydraulic conductivity of EC proppant-supported fractures decreases with increasing effective stress, which has been widely associated with stress-induced proppant embedment and compaction between opposing fracture surfaces, as reported in previous experimental and numerical studies (Chen et al., 2015; Fan et al., 2021; Li et al., 2022). The reduction in fracture hydraulic conductivity is most pronounced at 2,000 – 6,000 psi, particularly for partial-monolayer and multilayer proppant packs, due to progressive proppant embedment and compaction between the opposing granite slab surfaces. The fracture hydraulic conductivity did not change noticeably when the effective stress exceeded 6,000 psi, suggesting that proppant embedment and compaction had largely stabilized and that the proppant structure within the fracture became relatively steady under higher stress conditions. These tests showed that the fracture generally maintained adequate hydraulic conductivity under an effective stress of 10,000 psi with various proppant concentrations.

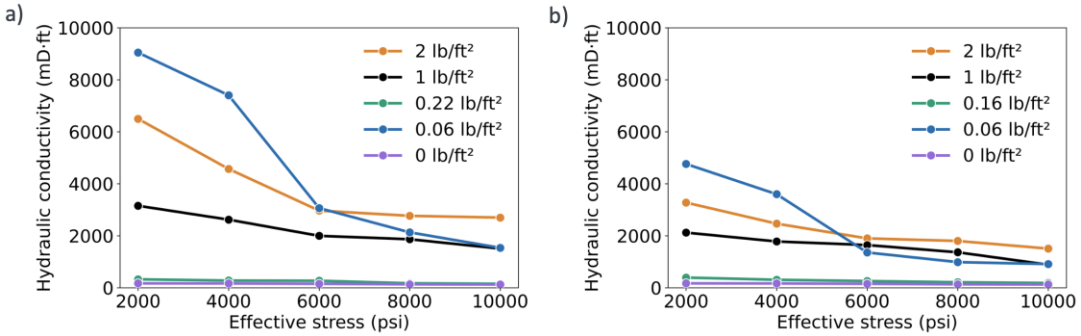

Figure 3: Laboratory-measured fracture's hydraulic conductivity of a) iON 30/50 EC proppants, and b) iON 40/70 EC proppants against effective stress at 230 °C.

Figure 4 presents the same dataset but illustrates the fracture's hydraulic conductivity against proppant concentration. The non-monotonic dependence of fracture hydraulic conductivity on the proppant concentration was observed. A local minimum in fracture hydraulic conductivity corresponded to full-monolayer proppant structures for 30/50-mesh and 40/70-mesh proppants, with concentrations of 0.22 and 0.16 lb/ft², respectively. By contrast, a local maximum in fracture hydraulic conductivity was observed for partial-monolayer proppant structures at 0.06 lb/ft² for both proppant sizes. At this concentration, proppant particles did not fully cover the fracture surfaces, resulting in higher fracture porosity and permeability, which in turn enhanced fracture hydraulic conductivity. Previous experimental investigations have demonstrated that partial-monolayer proppant packs can achieve fracture conductivities comparable to, or exceeding, those obtained with traditional multilayer proppant assemblies (Chen et al., 2008, 2009; Bestaoui-Spurr and Hudson, 2017; Fan et al., 2017; Wang et al., 2025). Fan et al. (2019) demonstrated that the non-monotonic evolution of fracture hydraulic conductivity results from a competing interplay between fracture permeability and fracture width during the transition from partial-monolayer to multilayer proppant packs, based on combined laboratory experiments with the discrete element method (DEM) and lattice Boltzmann (LB) method. The detailed evolutions of fracture width, porosity, permeability, and conductivity go through four distinct stages with the increasing proppant concentration, as summarized in Table 1.

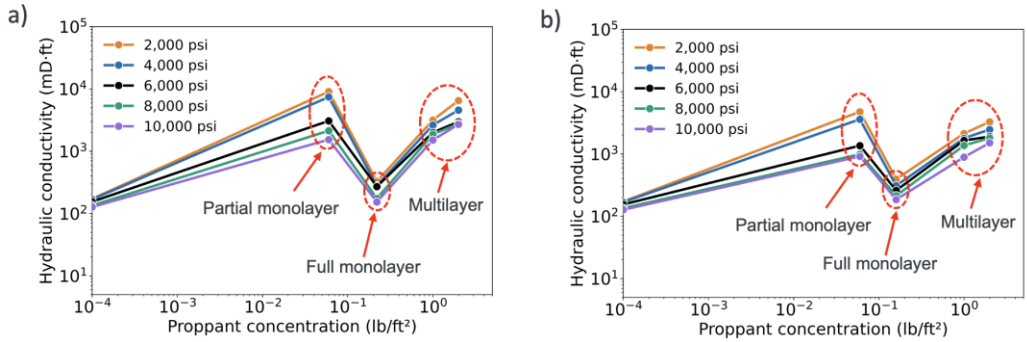

Figure 4: Laboratory-measured fracture's hydraulic conductivity of a) iON 30/50 EC proppants, and b) iON 40/70 EC proppants against proppant concentration at 230 °C.

Table 1: Evolutions of fracture width, w_f, porosity, φ, permeability, k, and fracture hydraulic conductivity, $k \cdot w_f$ with an increasing proppant concentration.

	w_f	φ	k	Hydraulic conductivity $(k \cdot w_f)$	Geometry of proppant pack
Stage 1	↑	↓	↑	↑	Partial monolayer
Stage 2	↑	↓	↓	↑	Partial monolayer
Stage 3	↑	↓	↓	↓	Partial monolayer to full monolayer
Stage 4	↑	→	→	↑	Full monolayer to multilayer

Note: The arrows "↑", "↓", and "→" denote "increase", "decrease", and "stay constant", respectively. The pattern is similar to those reported by Fan et al. (2019) and Li et al. (2022).

In Stage 1, the proppant concentration is low, and proppant embedment is initially significant. As additional proppant particles are introduced into the fracture, embedment is progressively mitigated, leading to an increase in fracture width and fracture permeability. Meanwhile, the increasing number of proppant particles occupies the available fracture void space, resulting in reduced fracture porosity,

which has a negative impact on permeability. Because the permeability gain associated with fracture widening exceeds the permeability loss caused by porosity reduction, the net effect is an increase in fracture permeability. Consequently, fracture hydraulic conductivity increases in this stage, as both fracture permeability and fracture width increase simultaneously.

In Stage 2, with further increases in proppant concentration, the permeability reduction caused by decreasing fracture porosity begins to exceed the permeability gain associated with fracture widening, leading to a gradual decline in fracture permeability. However, the reduction in permeability occurs at a slower rate than the increase in fracture width. As a result, fracture hydraulic conductivity, defined as the product of fracture permeability and fracture width, continues to increase during this stage.

In Stage 3, as proppant concentration continues to increase, the rate of permeability reduction eventually surpasses the rate of fracture width increase, causing fracture hydraulic conductivity to reach a local maximum and then begin to decline. The proppant concentration corresponding to this local maximum is defined as the optimal partial-monolayer proppant concentration, at which the fracture achieves its maximum fracture hydraulic conductivity, referred to as the optimal hydraulic conductivity of a fracture. This stage persists until the fracture surface becomes fully covered by a monolayer proppant pack.

In Stage 4, the proppant pack transitions from a full-monolayer structure to a multilayer structure. Once the fracture is filled with a densely packed proppant assembly, fracture porosity and permeability become primarily controlled by particle and pore-scale characteristics and are largely insensitive to further increases in fracture width. Consequently, fracture permeability and conductivity show limited variation with additional proppant loading.

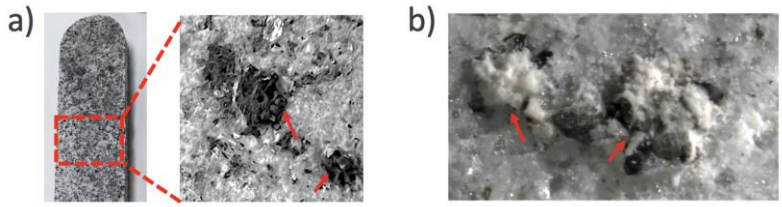

Figure 5: a) Embedded proppant particles and embedment impressions on granite surface, and b) a microscopic view revealing residual proppant particles partially embedded on the granite surface. Both pictures were observed after high-stress testing of EC proppants in partial-monolayer packs.

Figure 5 illustrates noticeable proppant embedment on the granite slab surfaces after high-stress testing of EC proppants in a partial-monolayer pack. This observation is consistent with previous laboratory studies (Chen et al., 2015; Fan et al., 2019, 2021; Li et al., 2022), which reported more pronounced embedment in partial-monolayer proppant packs compared to multilayer proppant packs due to higher localized loading on individual proppant particles. These results highlight the importance of considering proppant embedment when interpreting fracture hydraulic conductivity behavior in partial-monolayer proppant packs. Field studies have reported successful applications of partial-monolayer proppant structures (Posey and Strickland, 2005; Dahl et al., 2015). From both hydraulic and economic perspectives, such proppant packs are attractive, as they reduce material requirements while maintaining sufficient fracture hydraulic conductivity.

3.2 Electrical conductivity measurements under dry conditions

In this work, electrical conductivity measurements under dry conditions are used as a benchmark to isolate the effects of proppant packing structure and confining stress on conductive pathway development, serving as a reference for subsequent measurements under brine-saturated conditions. Figures 6a and 6b illustrate the fracture electrical resistivity of 30/50-mesh and 40/70-mesh proppants against confining stress under dry conditions at 230 °C. Across all proppant concentrations, the fractures propped by multilayer proppant packs (i.e., 1 and 2 lb/ft² for both 30/50-mesh and 40/70-mesh proppants) exhibited lower electrical resistivity than those propped by full-monolayer proppant packs (i.e., 0.22 lb/ft² for 30/50-mesh and 0.16 lb/ft² for 40/70-mesh), indicating the formation of more efficient conductive pathways when multiple proppant layers were present. This behavior can be interpreted using an equivalent-circuit analogy, where a multilayer proppant structure resembles a parallel network in which three-dimensional interparticle contacts provide multiple conductive pathways, resulting in lower electrical resistivity. In contrast, a full-monolayer proppant structure is analogous to a series network, where particles are primarily aligned in the horizontal direction, limiting the number of conductive pathways and resulting in higher electrical resistivity.

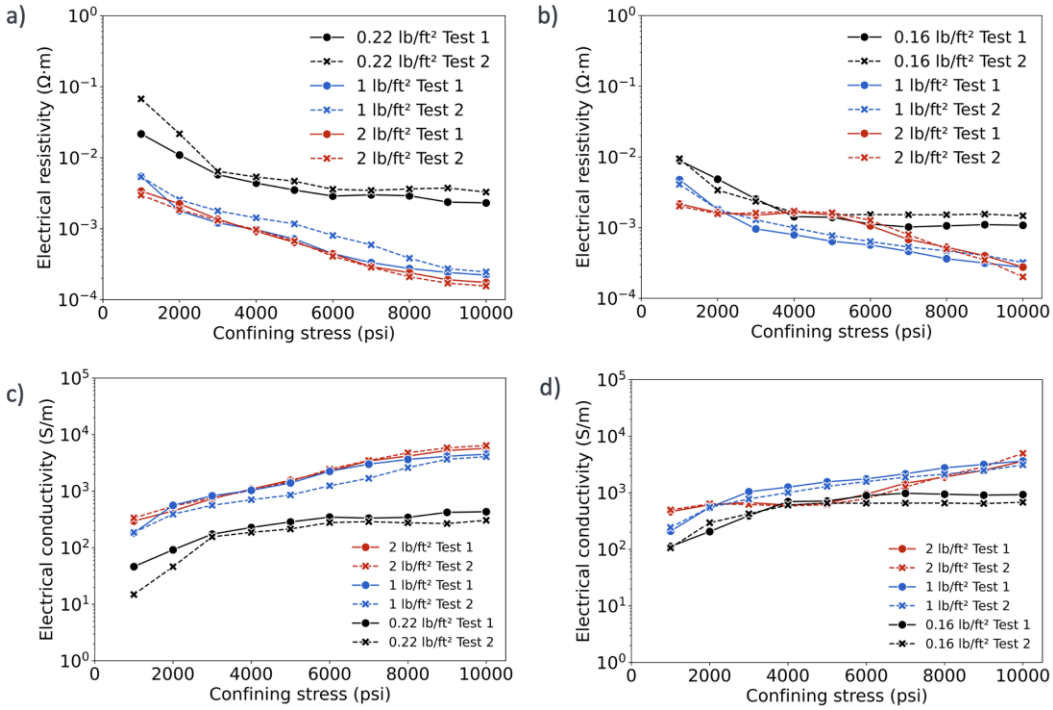

Figure 6: Laboratory-measured electrical resistivity of the fracture propped by a) iON 30/50 EC proppants, and b) iON 40/70 EC proppants, and the corresponding electrical conductivity of the fracture propped by c) iON 30/50 EC proppants, and d) iON 40/70 EC proppants, against confining stress under dry conditions at 230 °C.

In most cases, fractures propped by multilayer proppant packs exhibited a decrease in electrical resistivity with increasing confining stress, primarily due to compaction-induced reduction of interparticle pore space, which enhanced particle-to-particle contacts and promoted the formation of more effective conductive pathways. However, a notable exception was observed for the 40/70-mesh sample at 2 lb/ft². In this case, electrical resistivity exhibited a nonmonotonic trend between 3,000 and 6,000 psi, which was attributed to localized structural changes caused by particle rearrangement and detachment of metal coating on proppant surface, affecting the continuity of conductive pathways. At confining stresses above 6,000 psi, the electrical resistivity declined again, indicating that a stable and continuous interparticle conductive network had formed. In this stage, the enhanced interparticle contacts dominated electrical transport, outweighing the adverse effects caused by the detachment of metal coating.

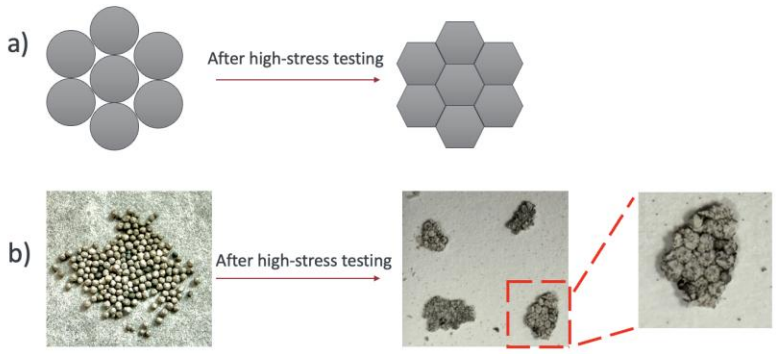

Figure 7: a) schematic illustration, and b) laboratory photos of EC proppants in a full-monolayer pack before and after high-stress testing, showing stress-induced aggregation and deformation of proppant particles.

Fractures propped by full-monolayer proppant packs exhibited a characteristic two-stage response in electrical resistivity to increasing confining stress. At stresses below approximately 6,000 psi, electrical resistivity decreases rapidly. This behavior was primarily controlled by particle deformation and aggregation, as shown in Figures 7a and 7b, which enlarged contact areas between adjacent proppant particles and progressively enhanced conductive network connectivity. In addition, the detached metal coating fragments under increasing stress bridged interparticle voids, further facilitating charge transport. Above 6,000 psi, the fracture electrical resistivity began to stabilize. At this stage, a stable and continuous conductive network had already formed, and further increases in confining stress contributed only marginally to additional improvements in network connectivity.

As shown in Figures 6c and 6d, under the highest applied confining stress of 10,000 psi, the EC proppant-supported fracture exhibited an electrical conductivity exceeding 200 S/m, more than five orders of magnitude higher than that of fractured granite without EC proppant (< 0.001 S/m) (Lockner and Byerlee, 1986; Gomaa, 2021). This result highlights the strong potential of EC proppants to generate highly conductive fracture networks suitable for borehole electromagnetic measurements.

4. CONCLUSION

This study presents a comprehensive laboratory investigation of the hydraulic and electrical conductivities of electrically-conductive (EC) proppant-supported fractures under stress and temperature conditions typical of the Utah-FORGE EGS. The results demonstrate the feasibility of using EC proppants to simultaneously sustain fracture hydraulic and electrical performance, thereby enabling effective borehole electromagnetic (EM) fracture diagnostics and supporting the optimization of fracture design and long-term performance in EGS reservoirs.

The hydraulic conductivity of EC proppant-supported fractures does not increase monotonically with proppant concentration. Instead, its evolution reflects a competition between fracture permeability and fracture width. As a result of this competing mechanism, an optimal proppant packing concentration emerges, at which partial-monolayer proppant packs can achieve conductivity levels comparable to, or even higher than, those of multilayer assemblies. This outcome carries important practical implications: high-strength EC proppants can sustain high fracture hydraulic conductivity while requiring substantially less material, thereby lowering material costs.

The electrical conductivity of EC proppant-supported fractures generally increases with confining stress under dry conditions at 230 ℃, as particle contacts progressively improve across different proppant concentrations and particle sizes. Stress-induced particle deformation, aggregation, and detachment of metal coating collectively affect interparticle contact characteristics and the continuity of conductive pathways. Overall, the EC proppant-supported granite fracture exhibits an electrical conductivity more than five orders of magnitude higher than that of fractured granite without EC proppant, indicating strong potential for detecting and delineating proppant-supported fractures in EGS formations using borehole electromagnetic (EM) measurements. Additionally, these dry-condition measurements provide a well-defined baseline for subsequent investigations under brine-saturated conditions, which is essential for realistically simulating fracture behavior in enhanced geothermal systems (EGS) reservoirs.

ACKNOWLEDGMENTS

The authors are thankful for the financial support provided by the U.S. Department of Energy (DOE) and the Utah Frontier Observatory for Research in Geothermal Energy (FORGE) under the award number of 9-3635. The authors also thank CARBO Ceramics for providing the EC proppants used in the laboratory tests.

REFERENCES

Al Balushi, F., Zhang, Q., Dahi Taleghani, A., 2023. Improving enhanced geothermal systems performance using adaptive fracture conductivity. Appl. Therm. Eng. 233, 121206. https://doi.org/10.1016/j.applthermaleng.2023.121206

Balushi, F.A., Taleghani, A.D., 2023. Thermally Conductive Proppants to Improve Heat Extraction in Geothermal Systems, in: SPE Annual Technical Conference and Exhibition. Presented at the SPE Annual Technical Conference and Exhibition, SPE, San Antonio, Texas, USA, p. D021S016R002. https://doi.org/10.2118/214824-MS

Bestaoui-Spurr, N., Hudson, H., 2017. Ultra-Light Weight Proppant and Pumping Design Lead to Greater Conductive Fracture Area in Unconventional Reservoirs, in: SPE Oil and Gas India Conference and Exhibition. Presented at the SPE Oil and Gas India Conference and Exhibition, SPE, Mumbai, India, p. D021S009R003. https://doi.org/10.2118/185435-MS

Chen, C., Lau, B.L.T., Gaillard, J., Packman, A.I., 2009. Temporal evolution of pore geometry, fluid flow, and solute transport resulting from colloid deposition. Water Resour. Res. 45, 2008WR007252. https://doi.org/10.1029/2008WR007252

Chen, C., Martysevich, V., O'Connell, P., Hu, D., Matzar, L., 2015. Temporal Evolution of the Geometrical and Transport Properties of a Fracture/Proppant System Under Increasing Effective Stress. SPE J. 20, 527–535. https://doi.org/10.2118/171572-PA

Chen, C., Packman, A.I., Gaillard, J., 2008. Pore-scale analysis of permeability reduction resulting from colloid deposition. Geophys. Res. Lett. 35, 2007GL033077. https://doi.org/10.1029/2007GL033077

Dahl, J., Nguyen, P., Dusterhoft, R., Calvin, J., Siddiqui, S., 2015. Application of Micro-Proppant to Enhance Well Production in Unconventional Reservoirs: Laboratory and Field Results, in: SPE Western Regional Meeting. Presented at the SPE Western Regional Meeting, SPE, Garden Grove, California, USA, p. SPE-174060-MS. https://doi.org/10.2118/174060-MS

Fan, M., Han, Y., McClure, J., Chen, C., 2017. Hydraulic Fracture Conductivity as a Function of Proppant Concentration Under Various Effective Stresses: From Partial Monolayer to Multilayer Proppants, in: Proceedings of the 5th Unconventional Resources Technology Conference. Presented at the Unconventional Resources Technology Conference, American Association of Petroleum Geologists, Austin, Texas, USA. https://doi.org/10.15530/urtec-2017-2693347

Fan, M., Li, Z., Han, Y., Teng, Y., Chen, C., 2021. Experimental and Numerical Investigations of the Role of Proppant Embedment on Fracture Conductivity in Narrow Fractures (includes associated Errata). SPE J. 26, 324–341. https://doi.org/10.2118/204222-PA

Fan, M., McClure, J., Han, Y., Ripepi, N., Westman, E., Gu, M., Chen, C., 2019. Using an Experiment/Simulation-Integrated Approach To Investigate Fracture-Conductivity Evolution and Non-Darcy Flow in a Proppant-Supported Hydraulic Fracture. SPE J. 24, 1912–1928. https://doi.org/10.2118/195588-PA

Gan, Q., Elsworth, D., 2016. Production optimization in fractured geothermal reservoirs by coupled discrete fracture network modeling. Geothermics 62, 131–142. https://doi.org/10.1016/j.geothermics.2016.04.009

Gomaa, M., 2021. Frequency response of electrical properties of some Granite samples. فیزیک زمین و فضا. https://doi.org/10.22059/jesphys.2021.318321.1007287

Gong, F., Guo, T., Sun, W., Li, Z., Yang, B., Chen, Y., Qu, Z., 2020. Evaluation of geothermal energy extraction in Enhanced Geothermal System (EGS) with multiple fracturing horizontal wells (MFHW). Renew. Energy 151, 1339–1351. https://doi.org/10.1016/j.renene.2019.11.134

Hoversten, G.M., Schwarzbach, C., 2021. Monitoring hydraulic fracture volume using borehole to surface electromagnetic and conductive proppant. GEOPHYSICS 86, E93–E109. https://doi.org/10.1190/geo2020-0410.1

Jolie, E., Scott, S., Faulds, J., Chambefort, I., Axelsson, G., Gutiérrez-Negrín, L.C., Regenspurg, S., Ziegler, M., Ayling, B., Richter, A., Zemedkun, M.T., 2021. Geological controls on geothermal resources for power generation. Nat. Rev. Earth Environ. 2, 324–339. https://doi.org/10.1038/s43017-021-00154-y

Ko, S.K., Ghassemi, A., Uddenberg, M., 2023. Selection and Testing of Proppants for EGS (No. SGP-TR-224), Proceedings, 48th Workshop on Geothermal Reservoir Engineering. Stanford University, Geothermal Program, Stanford, California, USA.

Li, D., Li, N., Jia, J., Yu, H., Fan, Q., Wang, L., Mohsen, A., 2024. Development status and research recommendations for thermal extraction technology in deep hot dry rock reservoirs. Deep Undergr. Sci. Eng. 3, 317–325. https://doi.org/10.1002/dug2.12080

Li, D., Wu, Y., Hao, Y., Ma, D., Yao, C., 2025. Experimental study on the shear behavior of propped rough fractures in geothermal reservoir. Geoenergy Sci. Eng. 247, 213698. https://doi.org/10.1016/j.geoen.2025.213698

Li, Z., Ripepi, N., Chen, C., 2020. Using pressure pulse decay experiments and a novel multi-physics shale transport model to study the role of Klinkenberg effect and effective stress on the apparent permeability of shales. J. Pet. Sci. Eng. 189, 107010. https://doi.org/10.1016/j.petrol.2020.107010

Li, Z., Ripepi, N., Chen, C., 2019. Comprehensive laboratory investigation and model fitting of klinkenberg effect and its role on apparent permeability in various US shale formations, in: Proceedings of the ARMA US Rock Mechanics/Geomechanics Symposium, ARMA-2019-1568. Presented at the 53rd U.S. Rock Mechanics/Geomechanics Symposium, American Rock Mechanics Association, New York, NY, USA.

Li, Z., Zhang, W., Tang, Y., Li, B., Song, Z., Hou, J., 2016. Formation damage during alkaline-surfactant-polymer flooding in the Sanan-5 block of the Daqing Oilfield, China. J. Nat. Gas Sci. Eng. 35, 826–835. https://doi.org/10.1016/j.jngse.2016.07.046

Li, Z., Zhao, Q., Teng, Y., Fan, M., Ripepi, N., Yin, X., Chen, C., 2022. Experimental investigation of non-monotonic fracture conductivity evolution in energy georeservoirs. J. Pet. Sci. Eng. 211, 110103. https://doi.org/10.1016/j.petrol.2022.110103

Liang, Y., Teng, B., Dai, D., Shi, J., 2025. Study of the Heat Extraction Performance of Integrated Enhanced Geothermal Systems Based on a Novel Semi-Analytical Model. SPE J. 30, 2107–2126. https://doi.org/10.2118/224439-PA

Liu, S., Ji, K., Jin, M., 2025. Review of Techniques to Mitigate Thermal Breakthrough in Enhanced Geothermal Systems. https://doi.org/10.20944/preprints202505.0422.v1

Lockner, D.A., Byerlee, J.D., 1986. Changes in complex resistivity during creep in granite. Pure Appl. Geophys. 124, 659–676. https://doi.org/10.1007/BF00879603

Meng, N., Xu, W., He, K., Gao, X., 2025. A novel multi-scale fully coupled method for simulation and lifecycle performance optimization of enhanced geothermal systems. Energy 341, 139554. https://doi.org/10.1016/j.energy.2025.139554

Nataša A. Kablar, 2019. Renewable Energy: Wind Turbines, Solar Cells, Small Hydroelectric Plants, Biomass, and Geothermal Sources of Energy. J. Energy Power Eng. 13. https://doi.org/10.17265/1934-8975/2019.04.004

Nath, F., Mahmood, M.N., Ofosu, E., Khanal, A., 2024. Enhanced geothermal systems: A critical review of recent advancements and future potential for clean energy production. Geoenergy Sci. Eng. 243, 213370. https://doi.org/10.1016/j.geoen.2024.213370

Palisch, T., Al-Tailji, W., Bartel, L., Cannan, C., Zhang, J., Czapski, M., Lynch, K., 2017. Far-Field Proppant Detection Using Electromagnetic Methods - Latest Field Results, in: SPE Hydraulic Fracturing Technology Conference and Exhibition. Presented at the SPE Hydraulic Fracturing Technology Conference and Exhibition, SPE, The Woodlands, Texas, USA, p. D011S001R001. https://doi.org/10.2118/184880-MS

Posey, D., Strickland, B., 2005. The Effect of Using a Lightweight Proppant in Treatment of a Low-Permeability, Dry Gas Reservoir: A Case Study, in: SPE Eastern Regional Meeting. Presented at the SPE Eastern Regional Meeting, SPE, Morgantown, West Virginia, p. SPE-97998-MS. https://doi.org/10.2118/97998-MS

Qu, H., Zeng, Z., Liu, Y., Zhou, M., Liu, Xu, Lu, Z., Wang, S., Liu, Xiaodong, Chen, X., 2024. Experimental and Simulation Investigations of Proppant Transport and Distribution Between Perforation Clusters in a Horizontal Well. SPE J. 29, 5286–5304. https://doi.org/10.2118/223087-PA

Ren, L., Lin, C., Zhao, J., Lin, R., Zhou, B., Wu, J., 2025. Simulation and analysis of proppant transportation and distribution rules under multi-cluster perforation in horizontal wellbore. Pet. Sci. Technol. 43, 3329–3352. https://doi.org/10.1080/10916466.2024.2414843

Suzuki, T., Yoshimura, R., Yamazaki, K., Minami, T., Sawayama, K., Oshiman, N., 2024. Dependence of resistivity of natural rock samples on humidity. J. Appl. Geophys. 220, 105271. https://doi.org/10.1016/j.jappgeo.2023.105271

Szanyi, J., Rybach, L., Abdulhaq, H.A., 2023. Geothermal Energy and Beyond—A Review. https://doi.org/10.20944/preprints202308.1267.v1

Tomac, I., Sauter, M., 2018. A review on challenges in the assessment of geomechanical rock performance for deep geothermal reservoir development. Renew. Sustain. Energy Rev. 82, 3972–3980. https://doi.org/10.1016/j.rser.2017.10.076

Wang, D., Zhang, J., Jiang, X., Feng, J., Wu, Y., Li, B., Lu, M., Pan, Z., 2025. Optimal packing ratio of proppant monolayer for partially-propped horizontal bedding fractures of shale. Gas Sci. Eng. 135, 205563. https://doi.org/10.1016/j.jgsce.2025.205563

Wu, S., Liu, D., Huang, W., Zhang, C., 2024. Characterization of electrically conductive hydrofractures with cross-borehole electromagnetic measurement. Acta Geophys. 73, 1593–1607. https://doi.org/10.1007/s11600-024-01478-1

Zhang, F., He, G., An, M., Huang, R., Elsworth, D., 2025. Permeability evolution of fluid-injection-reactivated granite fractures of contrasting roughnesses. Undergr. Space 20, 33–45. https://doi.org/10.1016/j.undsp.2024.02.007

Zhang, P., Ozowe, W., Russell, R.T., Sharma, M.M., 2021. Characterization of an electrically conductive proppant for fracture diagnostics. GEOPHYSICS 86, E13–E20. https://doi.org/10.1190/geo2019-0367.1